RESEARCH PAPER

TiO$_2$ nanoparticles on nitrogen-doped graphene as anode material for lithium ion batteries

**Dan Li · Dongqi Shi · Zongwen Liu ·
Huakun Liu · Zaiping Guo**

Abstract Anatase TiO$_2$ nanoparticles in situ grown on nitrogen-doped, reduced graphene oxide (rGO) have been successfully synthesized as an anode material for the lithium ion battery. The nanosized TiO$_2$ particles were homogeneously distributed on the reduced graphene oxide to inhibit the restacking of the neighbouring graphene sheets. The obtained TiO$_2$/N-rGO composite exhibits improved cycling performance and rate capability, indicating the important role of reduced graphene oxide, which not only facilitates the formation of uniformly distributed TiO$_2$ nanocrystals, but also increases the electrical conductivity of the composite material. The introduction of nitrogen on the reduced graphene oxide has been proved to increase the conductivity of the reduced graphene oxide and leads to more defects. A disordered structure is thus formed to accommodate more lithium ions, thereby further improving the electrochemical performance.

Keywords TiO$_2$ nanoparticles · Nitrogen-doped graphene · Hydrothermal reaction · Anode material · Lithium ion batteries

D. Li · D. Shi · H. Liu · Z. Guo (✉)
Institute for Superconducting and Electronic Materials, University of Wollongong, Wollongong, NSW 2522, Australia
e-mail: zguo@uow.edu.au

Z. Liu
School of Chemical and Biomolecular Engineering, The University of Sydney, Sydney, NSW, Australia

Z. Guo
School of Mechanical, Materials & Mechatronics Engineering, University of Wollongong, Wollongong, NSW 2522, Australia

Introduction

Metal oxides have been considered as a significant family of high-power anode materials for rechargeable lithium ion batteries (Poizot et al. 2000) because of their diverse chemical and physical properties, as well as their high reversible capacities. Recently, titanium dioxide has garnered huge attention because of its wide potential applications in sensing, photocatalysis, electronic devices, conversion devices, solar cells and energy storage (Subramanian et al. 2006; Han et al. 2011a), because of its abundance, low cost and environmental benignity (Wagemaker et al. 2002; Hu et al. 2006). In the field of lithium ion batteries, TiO$_2$ has been particularly studied, since it also has high potential, flat operating potential, a safe and stable structure with a negligible volume change (<4%) in the processes of lithium ion intercalation/de-intercalation and intrinsic safety because lithium electrochemical deposition can be avoided (Wang et al. 2009; Qiu et al. 2010). There are eight

polymorphs of TiO_2, among which, anatase is widely considered to be the most electroactive host for lithium ion insertion (Kavan et al. 1996).

The sluggish lithium ion diffusion and low-electronic conductivity ($\sim 10^{-13}$ s cm^{-1}) of TiO_2 are obstacles, however, to its practical application in higher power output applications. Nanomaterials have been employed to improve the electrochemical performance of TiO_2. It is reported that nanosheets (Liu et al. 2011), nanoribbons (Kim et al. 2009), nanotubes (Kim and Cho 2007) and nanowires (Wang et al. 2008) can shorten the diffusion length for lithium ions, provide good electronic transport paths, owing to the large surface to volume ratio and increase lithium transport between the electrode and electrolyte (Arico et al. 2005), thus enhancing the electrochemical performance. Nevertheless, another problem arising from the nanosized materials is the strong tendency toward aggregation of TiO_2 nanoparticles. Therefore, strategies such as introducing a conductive coating layer, decorating the nanoparticles on certain substrates and embedding the nanostructures in a conductive matrix have been applied to prevent nanostructures from aggregating and, more importantly, to increase the conductivity.

Recently, graphene-based electrode materials, such as Co_3O_4/graphene composites (Park et al. 2011; Wu et al. 2011a; Li et al. 2013), SnO_2/graphene nanoporous composites (Paek et al. 2008), MnO/graphene nanosheet hybrid (Zhang et al. 2012a) and $Li_4Ti_5O_{12}$/graphene composite (Zhu et al. 2010) have attracted considerable interest because of their improved rate capability and enhanced cyclic performance because of their high electrical conductivity, high surface areas, broad electrochemical window and chemical tolerance (Paek et al. 2008; Stankovich et al. 2006). It is also found that a graphene layer can effectively hinder severe aggregation of nanoparticles in charge/discharge processes (Wu et al. 2011a).

Chemical doping is expected to substantially increase the density of free charge carriers and thereby enhance the electrical conductivity (Rao et al. 1997). So far, nitrogen-doped graphene is widely studied to enhance the properties of electrode materials, as it shows improved capacity, cycle life and rate performance compared with pristine graphene (Wu et al. 2011b; Wang et al. 2012a). Its advantages are derived from the conjugation between the nitrogen lone-pair electrons and the graphene π system (Liu et al. 2010).

Notably, nitrogen doping can improve the conductivity, which can be attributed to the decreased semiconducting gap after doping and the appearance of a finite density of states at zero energy in the graphene (Mousavi and Moradian 2011), so that a band gap is opened up between the valence band and conduction band (Wang et al. 2012b). There is higher electronegativity around the sites of nitrogen doping on the graphene, which can attract a larger number of lithium ions and therefore enhance the capacity (Shin et al. 2012), as shown in Fig. 1a. Based on first-principles' calculations, the process of nitrogen doping can introduce more defects than is possible with pristine graphene, and the presence of vacancy defects can enhance the ratio of Li:C, which facilitates free lithium ion diffusion between the graphene sheets in a perpendicular direction (Fan et al. 2012). Owing to the presence of defects, the lithium ion can easily diffuse to the vacancy and then go through to the other surface of the graphene sheet or to the surface of another layer of graphene, because the diffusion barrier at the hexagonal sites around the defects is much lower than in pristine graphene (as shown in Fig. 1b) (Fan et al. 2012). Furthermore, Shin et al. (2012) believed that the nitrogen doping could introduce more favourable binding between nitrogen-doped sites and metal oxide nanoparticles, and play a critical role in assisting the good dispersion of nanoparticles during cycling. Moreover, nitrogen doping has been demonstrated to enhance the surface hydrophilicity to facilitate the electrolyte–electrode interactions (Wang et al. 2012b). There are three different types of nitrogen-doped graphene sheets: graphitic, pyridinic and pyrrolic graphene (Ma et al. 2012). The results of first-principles' calculations also show that the pyridinic graphene is the most suitable for lithium ion storage at high capacity (Ma et al. 2012), and this pyridinic nitrogen would increase the density of electronic states (DOEs) around the Fermi level and open up the band gap of graphene (Wang et al. 2010a). Up to now, there are only some studies reporting that nitrogen-doped graphene sheets as a conductive matrix material for electrode material deposition (Wang et al. 2012a), and to the best of our knowledge, there have been no reports on N-doped graphene/TiO_2 as anode material for lithium ion batteries.

In this study, a composite of TiO_2 nanoparticles attached to nitrogen-doped graphene sheets was synthesized as anode material for the lithium ion
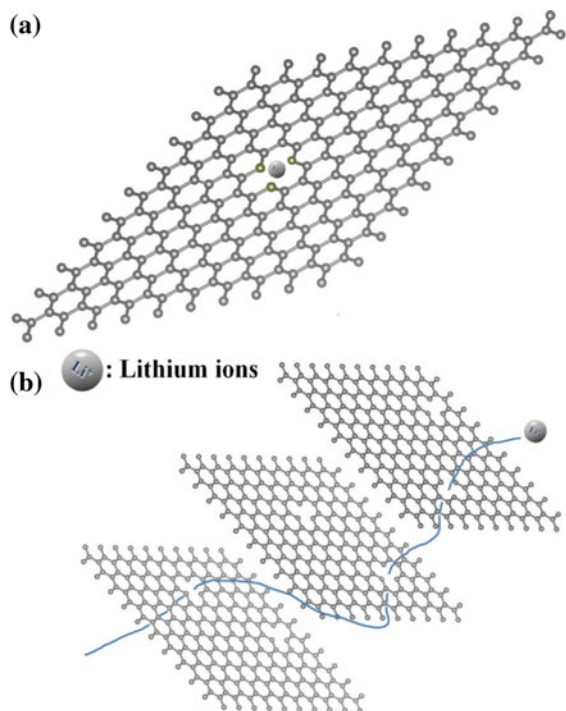
Fig. 1 Schematic drawings illustrating **a** the lithium ions inserting themselves into the defects on the graphene; **b** lithium ions diffuse through the defects on the graphene sheet from one side to another or to the side of another graphene sheet

battery, and the electrochemical properties were investigated to gain insight into the synergistic effects from the nitrogen doping on the graphene sheets. The nanosized-TiO_2 particles were uniformly distributed on the nitrogen-doped graphene sheets and therefore prevented the restacking of the graphene sheets. The nitrogen doping is proved to enhance the electrochemical performance of the composite material because of increased electronic conductivity, faster and easier lithium ion transfer across the graphene sheets, improved wettability between electrode and electrolyte, and more active sites provided for lithium storage on the graphene sheets. In addition, the good contact between TiO_2 nanoparticles and the nitrogen-doped graphene sheets can further improve electronic conductivity.

Experimental

Graphene oxide (GO) was synthesized from natural graphite powder by a modified Hummers method (Hummers and Offeman 1958; Li et al. 2008). 14 mg of the obtained GO was dispersed in 45-mL ethanol by ultrasonication for 0.5 h. 0.24-mL titanium(IV) iso-propoxide (97%, Aldrich) and 0.5 mL acetic acid (Aldrich) were mixed with 9.5-mL ethanol with stirring for 0.5 h. Then, the solution containing titanium precursor was added to the GO solution and then stirred for several hours at 80 °C to ensure a complete hydrolysis reaction. Subsequently, 0.2-mL hydrazine anhydrous (Aldrich) was added to the above solution with stirring for 20 min. Then, the solution was transferred into a Teflon-lined stainless steel reactor and heated at 200 °C for 20 h. After the reaction, a black powder was collected by centrifugation and washed with de-ionized water and ethanol several times before drying in an oven at 60 °C overnight. Samples of bare TiO_2 and TiO_2/reduced GO (rGO) were also prepared for comparison. The experimental steps for these samples were the same as for the synthesis of TiO_2/N-rGO, but without the GO for the bare TiO_2, and with the replacement of hydrazine by de-ionized water for TiO_2/rGO.

The crystalline phases of the resulting materials were analyzed by powder X-ray diffraction (XRD, MMA GBC, Australia), which was carried out using Cu Kα radiation ($\lambda = 1.54056$ Å) from $2\theta = 10°$ to 80°. Thermogravimetric analysis (TGA) was carried out to determine the carbon content with a TGA/ differential scanning calorimetry (DSC) type instrument (METTLER TOLEDO, Switzerland) at a heating rate of 10 °C min^{-1} from room temperature at 800 °C in air. Transmission electron microscope (TEM) investigations were performed using a JEOL 2011F analytical electron microscope (JEOL, Tokyo, Japan) operating at 200 keV. X-ray photoelectron spectroscopy (XPS) experiments were carried out on a VG Scientific ESCALAB 2201XL instrument using aluminium Kα X-ray radiation during XPS analysis. Raman spectra were collected in the range between 100 and 2,000 cm^{-1}.

To prepare the working electrode for electrochemical testing, a slurry was prepared by thoroughly mixing 80 wt% active material, 15 wt% acetylene black and 5 wt% poly(vinylidene fluoride) (PVdF) in *N*-methyl pyrrolidinone (NMP) solvent. The slurry was then spread onto copper foil substrates and dried in a vacuum oven at 120 °C for 3 h. The electrochemical tests were carried out on CR2032 coin-type cells. The cells were constructed of lithium foil as

anode, the prepared active material on copper as cathode, microporous polyethylene (Celgard 2400) as the separator and 1 M LiPF$_6$ in a mixture of ethylene carbonate (EC) and dimethyl carbonate (DMC) (1:1 by volume) as the electrolyte. The whole assembly process was carried out in an argon-filled glove box (Mbraun, Unilab, Germany). The charge/discharge cycling was performed within the voltage range of 1–3 V versus Li$^+$/Li on a battery test instrument (CT2001A, KINGNUO, China) at ambient temperature. Electrochemical impedance spectroscopy (EIS) was conducted by applying a dc potential equal to the open circuit voltage of the cell, with an amplitude of 5 mV over the frequency range from 100 kHz to 0.01 Hz.

Results and discussion

The crystal structures of TiO$_2$ and of the TiO$_2$/rGO and TiO$_2$/N-rGO composites were characterized through powder X-ray diffraction, as shown in Fig. 2. All three patterns can be indexed to the typical antatase TiO$_2$ structure with space group I4$_1$/amd (JCPDS card No. 21-1272). The strong and sharp peaks of TiO$_2$ show the good crystallinity and high purity of the obtained material (Qiu et al. 2010). In contrast, the diffraction peaks of the TiO$_2$/rGO and TiO$_2$/N-rGO composites have become broad and weak, indicating the small crystallite size. By applying Scherrer's equation to the (101) peak, the sizes of TiO$_2$, TiO$_2$/rGO and TiO$_2$/N-rGO particles were estimated to be 16, 13 and 12 nm, respectively, consistent with the results observed through the TEM images. It is worth pointing out that there is no peak attributed to rGO, suggesting that the TiO$_2$ nanoparticles separated the reduced graphene oxide sheets, preventing them from restacking and destroying the ordered structure (Yang et al. 2011). The TGA reveals that the amount of rGO in both TiO$_2$/N-rGO and TiO$_2$/rGO composites is about 17 %.

The phases of graphene and TiO$_2$ in the TiO$_2$/rGO and TiO$_2$/N-rGO composites were further confirmed through Raman spectra collected between 100 and 2,000 cm^{-1}, as shown in Fig. 3. The peak at 146 cm^{-1} is attributed to the E_g vibration mode of anatase (Saravanan et al. 2010; Cao et al. 2012). Besides the Raman-allowed phonon peak of TiO$_2$, there are two peaks centred at 1,333 cm^{-1}, denoted as the D band, corresponding to disordered carbon, and at
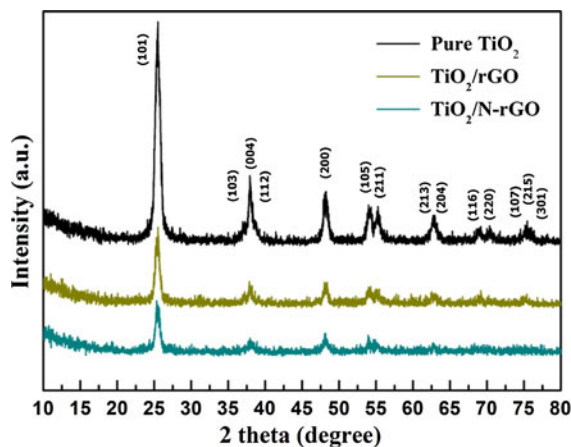
Fig. 2 Powder XRD patterns of bare TiO$_2$, and TiO$_2$/rGO and TiO$_2$/N-rGO composites

1,604 cm^{-1}, denoted as the G band, indicating the in-plane stretching motion of the symmetric sp^2-C band (Shen et al. 2009). The intensity ratio of the D band to the G band (I_D/I_G) is calculated to show the degree of disorder of the TiO$_2$/rGO and TiO$_2$/N-rGO composites originating from defects. Note that the intensity ratio for the TiO$_2$/N-rGO (1.6678) is much higher than that for the TiO$_2$/rGO (1.2339), which indicates that there are more defects in the rGO after nitrogen doping. It has been reported that the G band shift in chemically doped graphene provides information on the charge transfer between the dopants and the graphene (Rao et al. 1997; Kitaura et al. 2008). From Fig. 3b, it can be found that there is a redshift of the G peak, from 1,604 cm^{-1} for TiO$_2$/rGO to 1,592 cm^{-1} for TiO$_2$/N-rGO, suggesting that charge transfer has occurred from TiO$_2$ to the graphene sheets (Zhou et al. 2012).

The typical morphology and structure of the as-prepared TiO$_2$/N-rGO composite were observed via field emission scanning electron microscopy (FE-SEM) and transmission electron microscopy (TEM). It can be seen from Fig. 4a that TiO$_2$ nanoparticles are closely anchored onto the surfaces of the nitrogen-doped graphene sheets. The TEM images shown in Fig. 4b and c reveal that the nanoparticles which have a size range of 10–15 nm are uniformly attached on the graphene layers during the hydrothermal reaction process. The unique structure can improve electron transport through the nanoparticles and the graphene sheets, and thus improve the electrochemical performance of the composite. From TEM observation of the
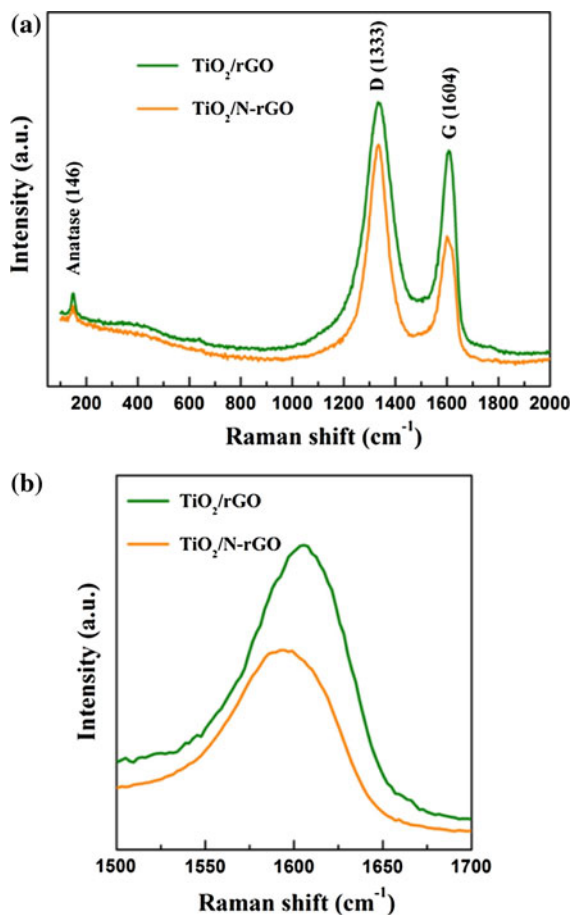
Fig. 3 a Raman spectra of TiO$_2$/rGO and TiO$_2$/N-rGO composites, **b** enlarged G band of TiO$_2$/rGO and TiO$_2$/N-rGO composites

bare TiO$_2$ (Fig S2a and b, Supporting Information), numerous fine nanoparticles with crystallite size of around 30 nm have grown together. The smaller particle size of TiO$_2$/N-rGO indicates that the presence of the graphene sheets could restrain the growth and aggregation of particles. In the high resolution TEM (HRTEM) image (shown in Fig. 4d), the periodic fringes of graphene and TiO nanoparticles can be clearly observed, which further confirms the high crystallinity of TiO$_2$. The crystal lattice fringes with *d*-spacing of 0.35 nm are characteristic of (101) lattice planes, which are the most stable and frequently observed in anatase TiO$_2$.

The XPS spectra reveal valuable information on the surface composition and functional groups on the TiO$_2$/N-rGO composite, as shown in Fig. 5. The Ti 2p spectrum for the composite comprises two peaks with binding energies of 459.6 and 465.6 eV, attributed to Ti 2p$_{3/2}$ and Ti 2p$_{1/2}$, respectively, which are typically Ti^{4+} in an octahedral environment (Qiu et al. 2010). The high-resolution XPS spectrum of C 1s in TiO$_2$/N-rGO can be deconvoluted into three peaks, as shown in Fig. 5a, which are centered at 284.8, 286.2 and 288.7 eV, corresponding to sp^2 hybridized carbon, alcohol or ether carbon, and carboxyl or ester carbon, respectively (Kim et al. 2012; Han et al. 2011b). In the O 1s XPS spectrum (shown in Fig. 5c), the main peak centered at 530.8 eV is assigned to oxygen in TiO$_2$ (Mo and Ye 2009), and the other peak at 532.6 eV can be attributed to ether (Kim et al. 2012). In terms of nitrogen, the energy feature at 398.6 eV is ascribed to the pyridinic N. It was reported that the electron deficiency causes graphene with a high defect content to have an electron-accepting tendency in the pyridinic structure, which allows it to store more lithium ions (Zhang et al. 2012a; Wang et al. 2012a; Ma et al. 2012).

In order to elucidate the effects of the rGO and nitrogen doping on the electrochemical performance, a series of electrochemical tests have been conducted. The rate capabilities of bare TiO$_2$, and the TiO$_2$/rGO and TiO$_2$/N-rGO composites are shown in Fig. 6a. The average reversible capacities of bare TiO$_2$, TiO$_2$/rGO and TiO$_2$/N-rGO are 194, 210 and 226 mA h g^{-1}, respectively, at a current rate of 0.2 C. The 1 C applied current was calculated based on the theoretical capacity of anatase TiO$_2$ for the change to Li$_{0.5}$TiO$_2$. It is clear that the capacities of TiO$_2$/rGO and TiO$_2$/N-rGO only slightly decrease with increasing cycle number, whereas the capacity of bare TiO$_2$ keeps fading from the initial 347.3 to 154.4 mA h g^{-1} after ten cycles. This phenomenon can be ascribed to the good electronic conductivity induced by graphene, which offers transfer channels for electrons and inhibits the aggregation of nanosized-TiO$_2$ particles. The higher capacities for all the three samples at 0.2 C than the theoretical value of TiO$_2$ could be attributed to the further lithium insertion in the surface layer of the obtained nanostructured particles (Borghols et al. 2009). For the samples of TiO$_2$/rGO and TiO$_2$/N-rGO, the higher capacities suggest the existence of additional lithium storage sites in or between the TiO$_2$/rGO sheets and defects after nitrogen doping, respectively. The following reversible capacities of TiO$_2$/rGO and TiO$_2$/N-rGO composite at different current rates are 172 mA h g^{-1} and 187 mA h g^{-1} at 1 C,

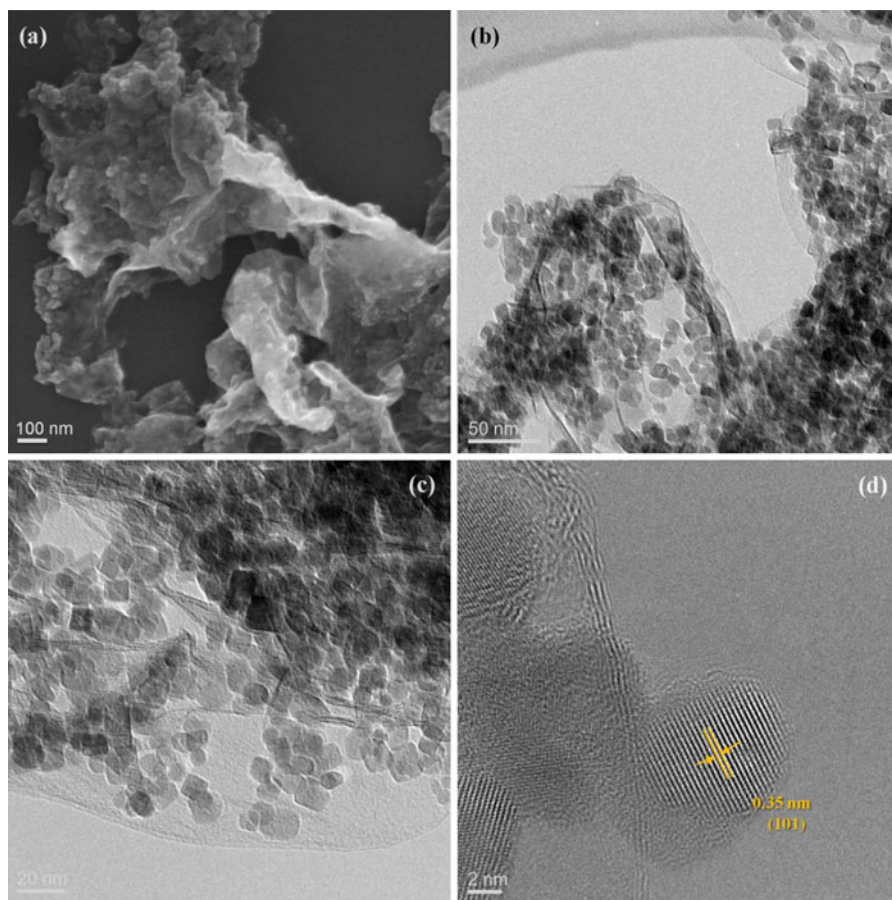**Fig. 4** **a** FE-SEM image, **b** and **c** TEM images and **d** HRTEM image of TiO_2/N-rGO composite

140 mA h g^{-1} and 148 mA h g^{-1} at 5 C, 110 mA h g^{-1} and 128 mA h g^{-1} at 10 C, and 85 mA h g^{-1} and 97 mA h g^{-1} at 20 C, respectively. The rate capability of our TiO_2/N-rGO is better than that of the TiO_2–graphene nanocomposite reported by Cai et al. (2012) and the sandwich-like, graphene-based titania nanosheets reported by Yang et al. (2011), as well as the electrospun TiO_2–graphene composite nanofibers reported by Zhang et al. (2012b). In addition, the TiO_2/rGO and TiO_2/N-rGO recover their initial capacities when the current density returns to 0.2 C, indicating the good reversibility of both samples. The first cycle galvanostatic discharge/charge profiles for TiO_2/rGO and TiO_2/N-rGO composite over the voltage range from 1 to 3 V are shown in Fig. 6b. The TiO_2/N-rGO exhibits a coulombic efficiency of 70.5 % at the initial cycle, which is higher than that of TiO_2/rGO (67.5 %). According to the reversible reaction of anatase TiO_2, the coefficient

value is 0.5 to form $Li_{0.5}TiO_2$ during the lithium insertion/extraction process, and the corresponding capacity is 167.5 mA h g^{-1} (Kim et al. 2009; Wagemaker et al. 2004). It is worth noting that the discharge capability at the first cycle at a current rate of 0.2 C is 319.4 and 299.5 mA h g^{-1}, suggesting that lithium-rich $Li_{0.95}TiO_2$ phase and $Li_{0.89}TiO_2$ phase have been formed for the TiO_2/N-rGO and TiO_2/rGO composite electrodes, respectively. The higher coefficient value indicates the existence of additional lithium storage sites in the TiO_2/N-rGO composite (Yang et al. 2011), which arise from the greater amount of defects formed after nitrogen doping. The discharge plateau at about 1.7 V corresponds to the lithium storage reaction between tetragonal anatase TiO_2 and orthorhombic $Li_{0.5}TiO_2$, whereas the charge plateau at about 2.0 V is related to the lithium extraction from $Li_{0.5}TiO_2$.

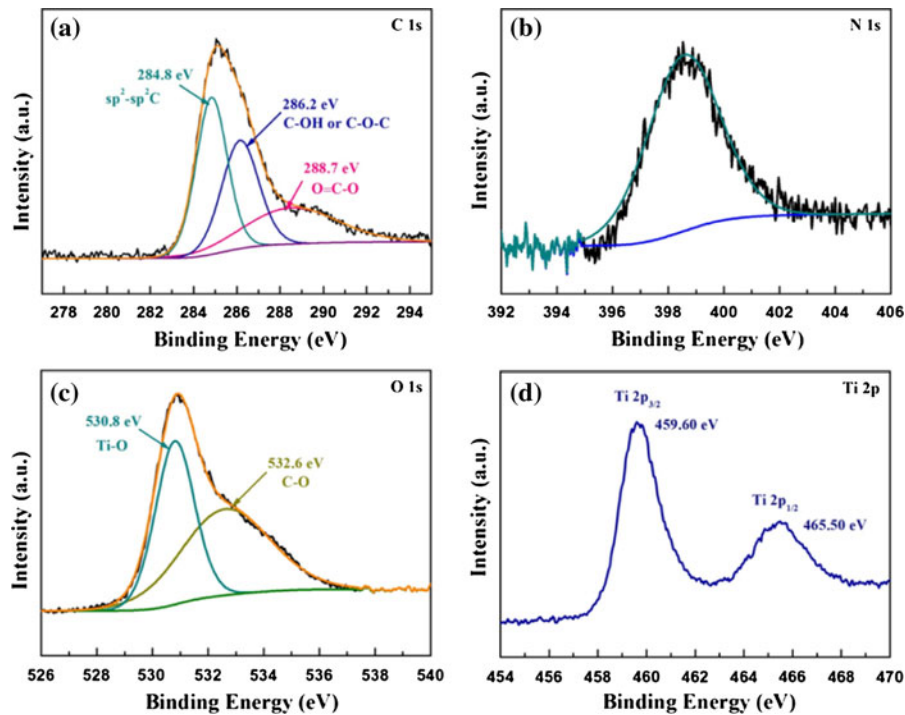In order to further evaluate the influence of nitrogen doping on the capacity retention properties, a

Fig. 5 XPS spectra of all elements of the TiO$_2$/N-rGO sample

relatively high current rate of 5 C was applied to the TiO$_2$/rGO and TiO$_2$/N-rGO electrodes. It can be observed that the capacities of both are almost same value of 175 mA h g^{-1} in the initial cycle. With increasing cycle number, the TiO$_2$/rGO composite maintains a capacity of 145 mA h g^{-1} for the first 45 cycles and then decreases to 133 mA h g^{-1} by the 70th cycle. In contrast, the TiO$_2$/N-rGO composite still maintain its reversible capacity of 153 mA h g^{-1} during the 70 cycles, which is higher and more stable performance than that of TiO$_2$/rGO. The improved cycling performance of TiO$_2$/N-rGO compared with TiO$_2$/rGO can be attributed to the nitrogen doping, which features good interfacial interaction and therefore gives rise to a stronger synergistic effect between the doped rGO and the TiO$_2$ nanoparticles than the bare-reduced graphene oxide (Wu et al. 2011a; Wang et al. 2010b). To further confirm the effects of nitrogen doping on the remarkable rate capability, EIS was carried out at ambient temperature, and the typical Nyquist plots of bare TiO$_2$, TiO$_2$/rGO and TiO$_2$/N-rGO are shown in Fig. 7. In the high-medium frequency region, the diameter of the semicircle for TiO$_2$/N-rGO is apparently much smaller than those of the bare TiO$_2$ and TiO$_2$/rGO. The reduced charge-

transfer resistance can be attributed to the enhanced electronic conductivity of the nitrogen-doped electrode that originates from graphene and nitrogen doping, which also improves the electrochemical activity of TiO$_2$ in the cycling process (Yang et al. 2011).

The reduced graphene oxide in the as-prepared composites plays a significant role in the improved electrochemical performance. On the one hand, the TiO$_2$ nanoparticles nucleate and grow directly on the reduced graphene oxide, which can further inhibit the growth and aggregation of TiO$_2$ nanoparticles. The good connection can maintain the integrity of the electrode during the charge and discharge processes, which is responsible for the high rate capability and cycling stability. On the other hand, the graphene sheets serve as an electronic network for the homogeneous TiO$_2$ nanoparticles, so as to achieve a good synergistic effect to improve the electronic conductivity. In addition, the uniformly distributed nanoparticles prevent the neighbouring graphene sheets from restacking, which can maximize the utilization of active material in the electrode. In terms of the effects of nitrogen doping on the electrochemical performance, firstly, the obtained pyridinic graphene sheets
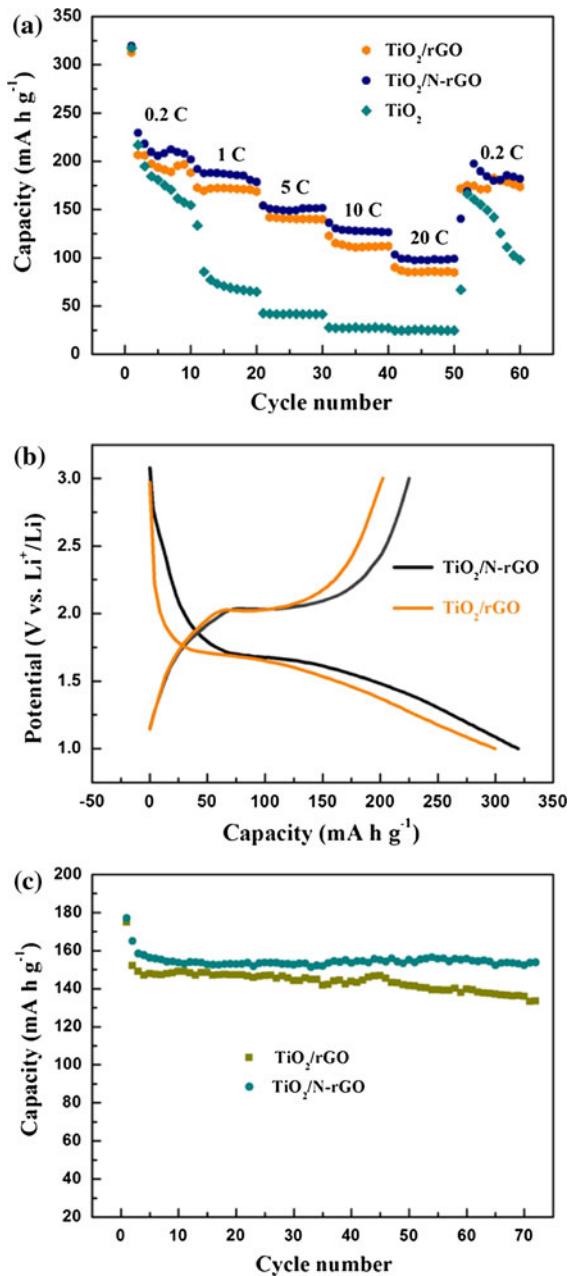
Fig. 7 Electrochemical impedance spectra of bare TiO_2, TiO_2/rGO and TiO_2/N-rGO composites

2012b). Thirdly, nitrogen doping could introduce defects on the graphene sheets to form a disordered carbon structure, which can increase the Li:C ratio, and therefore facilitate free lithium ion diffusion from one side of a graphene sheet to the other or between sheets. Moreover, the good wettability of the electrolyte–electrode interface (Wang et al. 2012b) after nitrogen doping and favourable binding between nitrogen-doped sites and lithium ions play a significant role in the improved electrochemical performance.

Conclusions

In summary, TiO_2/N-rGO composite was obtained through TiO_2 nanoparticle nucleation and growth on nitrogen-doped graphene. The graphene sheets not only prevent the aggregation of TiO_2 nanoparticles, but also provide increased electrical conductivity. The TiO_2/rGO and TiO_2/N-rGO composites exhibit excellent lithium storage performance, with high reversible capacity, improved rate capability, and superior cycling retention compared with bare TiO_2. In addition, the nitrogen doping increases the electronic conductivity of the graphene sheets, stabilizes the TiO_2 nanoparticles on the surface of the graphene and introduces more defects to store lithium ions. Therefore, this combination strategy enables the TiO_2/N-rGO composite to be a promising anode material for lithium ion batteries.

Fig. 6 **a** Comparison of rate capability of bare TiO_2, and TiO_2/rGO and TiO_2/N-rGO composites at various current rates from 0.2 to 20 C for 10 cycles; **b** first cycle discharge–charge *curves* for TiO_2/rGO and TiO_2/N-rGO composites at a current rate of 0.2 C; **c** comparison of the cycling performance of TiO_2/rGO and TiO_2/N-rGO at a constant current drain of 5 C

have defects at suitable sites for lithium ion storage. Secondly, the nitrogen doping improves the conductivity due to the band gap that is opened up between the valence band and the conduction band (Wang et al.
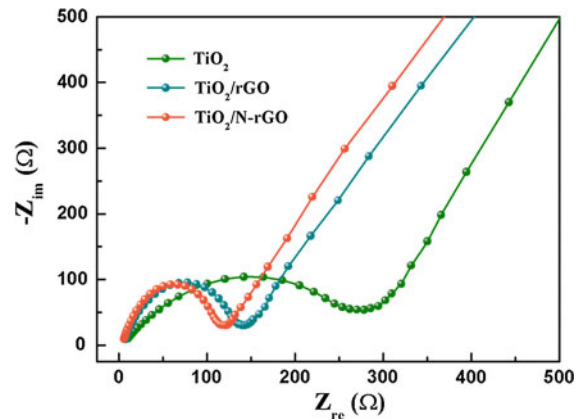
References

Arico AS, Bruce P, Scrosati B, Tarascon J-M, van Schalkwijk W (2005) Nanostructured materials for advanced energy conversion and storage devices. Nat Mater 4(5):366–377. doi:10.1038/nmat1368

Borghols WJH, Lutzenkirchen-Hecht D, Haake U, van Eck ERH, Mulder FM, Wagemaker M (2009) The electronic structure and ionic diffusion of nanoscale $LiTiO_2$ anatase. PCCP 11(27):5742–5748

Cai D, Lian P, Zhu X, Liang S, Yang W, Wang H (2012) High specific capacity of TiO_2–graphene nanocomposite as an anode material for lithium-ion batteries in an enlarged potential window. Electrochim Acta 74:65–72. doi:10.1016/j.electacta.2012.03.170

Cao H, Li B, Zhang J, Lian F, Kong X, Qu M (2012) Synthesis and superior anode performance of TiO_2@reduced graphene oxide nanocomposites for lithium ion batteries. J Mater Chem 22(19):9759–9766. doi:10.1039/C2JM00007E

Fan X, Zheng WT, Kuo J-L (2012) Adsorption and diffusion of Li on pristine and defective graphene. ACS Appl Mater Interfaces 4(5):2432–2438. doi:10.1021/am3000962

Han H, Song T, Bae J-Y, Nazar LF, Kim H, Paik U (2011a) Nitridated TiO_2 hollow nanofibers as an anode material for high power lithium ion batteries. Energy Environ Sci 4(11):4532–4536. doi:10.1039/C1EE02333K

Han P, Yue Y, Liu Z, Xu W, Zhang L, Xu H, Dong S, Cui G (2011b) Graphene oxide nanosheets/multi-walled carbon nanotubes hybrid as an excellent electrocatalytic material towards VO^{2+}/VO_2^+ redox couples for vanadium redox flow batteries. Energy Environ Sci 4(11):4710–4717. doi:10.1039/C1EE01776D

Hu YS, Kienle L, Guo YG, Maier J (2006) High lithium electroactivity of nanometer-sized rutile TiO_2. Adv Mater 18(11):1421–1426. doi:10.1002/adma.200502723

Hummers WS, Offeman RE (1958) Preparation of graphitic oxide. J Am Chem Soc 80(6):1339. doi:10.1021/ja01539a017

Kavan L, Grätzel M, Gilbert SE, Klemenz C, Scheel HJ (1996) Electrochemical and photoelectrochemical investigation of single-crystal anatase. J Am Chem Soc 118(28):6716–6723. doi:10.1021/ja954172l

Kim J, Cho J (2007) Rate characteristics of anatase TiO_2 nanotubes and nanorods for lithium battery anode materials at room temperature. J Electrochem Soc 154(6):A542–A546. doi:10.1149/1.2724756

Kim S-W, Han TH, Kim J, Gwon H, Moon H-S, Kang S-W, Kim SO, Kang K (2009) Fabrication and electrochemical characterization of TiO_2 three-dimensional nanonetwork based on peptide assembly. ACS Nano 3(5):1085–1090. doi:10.1021/nn900062q

Kim CH, Kim B-H, Yang KS (2012) TiO_2 nanoparticles loaded on graphene/carbon composite nanofibers by electrospinning for increased photocatalysis. Carbon 50(7):2472–2481. doi:10.1016/j.carbon.2012.01.069

Kitaura R, Imazu N, Kobayashi K, Shinohara H (2008) Fabrication of metal nanowires in carbon nanotubes via versatile nano-template reaction. Nano Lett 8(2):693–699. doi:10.1021/nl073070d

Li D, Muller MB, Gilje S, Kaner RB, Wallace GG (2008) Processable aqueous dispersions of graphene nanosheets. Nat Nano 3(2):101–105. doi:10.1038/nnano.2007.451

Li D, Shi D, Chen Z, Liu H, Jia D, Guo Z (2013) Enhanced rate performance of cobalt oxide/nitrogen doped graphene composite for lithium ion batteries. RSC Adv 3(15):5003–5008

Liu R, Wu D, Feng X, Müllen K (2010) Nitrogen-doped ordered mesoporous graphitic arrays with high electrocatalytic activity for oxygen reduction. Angew Chem Int Ed 49(14):2565–2569. doi:10.1002/anie.200907289

Liu J, Chen JS, Wei X, Lou XW, Liu X-W (2011) Sandwich-like, stacked ultrathin titanate nanosheets for ultrafast lithium storage. Adv Mater 23(8):998–1002. doi:10.1002/adma.201003759

Ma C, Shao X, Cao D (2012) Nitrogen-doped graphene nanosheets as anode materials for lithium ion batteries: a first-principles study. J Mater Chem 22(18):8911–8915. doi:10.1039/C2JM00166G

Mo D, Ye D (2009) Surface study of composite photocatalyst based on plasma modified activated carbon fibers with TiO_2. Surf Coat Technol 203(9):1154–1160. doi:10.1016/j.surfcoat.2008.10.007

Mousavi H, Moradian R (2011) Nitrogen and boron doping effects on the electrical conductivity of graphene and nanotube. Solid State Sci 13(8):1459–1464. doi:10.1016/j.solidstatesciences.2011.03.008

Paek S-M, Yoo E, Honma I (2008) Enhanced cyclic performance and lithium storage capacity of SnO_2/graphene nanoporous electrodes with three-dimensionally delaminated flexible structure. Nano Lett 9(1):72–75. doi:10.1021/nl802484w

Park M-H, Cho Y, Kim K, Kim J, Liu M, Cho J (2011) Germanium nanotubes prepared by using the Kirkendall effect as anodes for high-rate lithium batteries. Angew Chem Int Ed 50(41):9647–9650. doi:10.1002/anie.201103062

Poizot P, Laruelle S, Grugeon S, Dupont L, Tarascon JM (2000) Nano-sized transition-metal oxides as negative-electrode materials for lithium-ion batteries. Nature 407(6803):496–499. doi:10.1038/35035045

Qiu Y, Yan K, Yang S, Jin L, Deng H, Li W (2010) Synthesis of size-tunable anatase TiO_2 nanospindles and their assembly into anatase@titanium oxynitride/titanium nitride–graphene nanocomposites for rechargeable lithium ion batteries with high cycling performance. ACS Nano 4(11):6515–6526. doi:10.1021/nn101603g

Rao AM, Eklund PC, Bandow S, Thess A, Smalley RE (1997) Evidence for charge transfer in doped carbon nanotube bundles from Raman scattering. Nature 388(6639):257–259

Saravanan K, Ananthanarayanan K, Balaya P (2010) Mesoporous TiO_2 with high packing density for superior lithium storage. Energy Environ Sci 3(7):939–948. doi:10.1039/C003630G

Shen J, Hu Y, Shi M, Lu X, Qin C, Li C, Ye M (2009) Fast and facile preparation of graphene oxide and reduced graphene oxide nanoplatelets. Chem Mater 21(15):3514–3520. doi:10.1021/cm901247t

Shin WH, Jeong HM, Kim BG, Kang JK, Choi JW (2012) Nitrogen-doped multiwall carbon nanotubes for lithium storage with extremely high capacity. Nano Lett 12(5):2283–2288. doi:10.1021/nl3000908

Stankovich S, Dikin DA, Dommett GHB, Kohlhaas KM, Zimney EJ, Stach EA, Piner RD, Nguyen ST, Ruoff RS (2006) Graphene-based composite materials. Nature 442(7100): 282–286. doi:10.1038/nature04969

Subramanian V, Karki A, Gnanasekar KI, Eddy FP, Rambabu B (2006) Nanocrystalline TiO_2 (anatase) for Li-ion batteries. J Power Sour 159(1):186–192. doi:10.1016/j.jpowsour.2006.04.027

Wagemaker M, Kentgens APM, Mulder FM (2002) Equilibrium lithium transport between nanocrystalline phases in intercalated TiO_2 anatase. Nature 418(6896):397–399. doi:10.1038/nature00901

Wagemaker M, van Well AA, Kearley GJ, Mulder FM (2004) The life and times of lithium in anatase TiO_2. Solid State Ionics 175(1–4):191–193. doi:10.1016/j.ssi.2003.11.030

Wang Y, Wu M, Zhang WF (2008) Preparation and electrochemical characterization of TiO_2 nanowires as an electrode material for lithium-ion batteries. Electrochim Acta 53(27):7863–7868. doi:10.1016/j.electacta.2008.05.068

Wang D, Choi D, Li J, Yang Z, Nie Z, Kou R, Hu D, Wang C, Saraf LV, Zhang J, Aksay IA, Liu J (2009) Self-assembled TiO_2–graphene hybrid nanostructures for enhanced Li-ion insertion. ACS Nano 3(4):907–914. doi:10.1021/nn900150y

Wang Y, Shao Y, Matson DW, Li J, Lin Y (2010a) Nitrogen-doped graphene and its application in electrochemical biosensing. ACS Nano 4(4):1790–1798. doi:10.1021/nn100315s

Wang H, Cui L-F, Yang Y, Sanchez Casalongue H, Robinson JT, Liang Y, Cui Y, Dai H (2010b) Mn_3O_4–graphene hybrid as a high-capacity anode material for lithium ion batteries. J Am Chem Soc 132(40):13978–13980. doi:10.1021/ja105296a

Wang X, Cao X, Bourgeois L, Guan H, Chen S, Zhong Y, Tang D-M, Li H, Zhai T, Li L, Bando Y, Golberg D (2012a) N-doped graphene–SnO_2 sandwich paper for high-performance lithium-Ion batteries. Adv Funct Mater 22(13):2682–2690. doi:10.1002/adfm.201103110

Wang H, Maiyalagan T, Wang X (2012b) Review on recent progress in nitrogen-doped graphene: synthesis, characterization, and its potential applications. ACS Catal 2(5):781–794. doi:10.1021/cs200652y

Wu Z-S, Ren W, Wen L, Gao L, Zhao J, Chen Z, Zhou G, Li F, Cheng H-M (2011a) Graphene anchored with Co_3O_4 nanoparticles as anode of lithium ion batteries with enhanced reversible capacity and cyclic performance. ACS Nano 4(6):3187–3194. doi:10.1021/nn100740x

Wu Z-S, Ren W, Xu L, Li F, Cheng H-M (2011b) Doped graphene sheets as anode materials with superhigh rate and large capacity for lithium ion batteries. ACS Nano 5(7):5463–5471. doi:10.1021/nn2006249

Yang S, Feng X, Müllen K (2011) Sandwich-like, graphene-based titania nanosheets with high surface area for fast lithium storage. Adv Mater 23(31):3575–3579. doi:10.1002/adma.201101599

Zhang K, Han P, Gu L, Zhang L, Liu Z, Kong Q, Zhang C, Dong S, Zhang Z, Yao J, Xu H, Cui G, Chen L (2012a) Synthesis of nitrogen-doped MnO/graphene nanosheets hybrid material for lithium ion batteries. ACS Appl Mater Interfaces 4(2):658–664. doi:10.1021/am201173z

Zhang X, Suresh Kumar P, Aravindan V, Liu HH, Sundaramurthy J, Mhaisalkar SG, Duong HM, Ramakrishna S, Madhavi S (2012b) Electrospun TiO_2–graphene composite nanofibers as a highly durable insertion anode for lithium ion batteries. J Phys Chem C 116(28):14780–14788. doi:10.1021/jp302574g

Zhou G, Wang D-W, Yin L-C, Li N, Li F, Cheng H-M (2012) Oxygen bridges between NiO nanosheets and graphene for improvement of lithium storage. ACS Nano 6(4): 3214–3223. doi:10.1021/nn300098m

Zhu N, Liu W, Xue M, Xie Z, Zhao D, Zhang M, Chen J, Cao T (2010) Graphene as a conductive additive to enhance the high-rate capabilities of electrospun $Li_4Ti_5O_{12}$ for lithium-ion batteries. Electrochim Acta 55(20):5813–5818. doi:10.1016/j.electacta.2010.05.029